physica status solidi b

phys. stat. sol. (b) **244**, No. 3, 866–882 (2007) / **DOI** 10.1002/pssb.200572706

Auxetic behaviour from rotating semi-rigid units

J. N. Grima[*, 1], **V. Zammit**[1], **R. Gatt**[1], **A. Alderson**[2], and **K. E. Evans**[3]

[1] Department of Chemistry, University of Malta, Msida MSD 06, Malta
[2] Centre for Materials Research and Innovation, University of Bolton, Bolton BL3 5AB, UK
[3] Department of Engineering, University of Exeter, Exeter EX4 4QF, UK

Received 30 September 2005, accepted 28 August 2006
Published online 18 January 2007

PACS 31.15.Qg, 62.20.+e

Auxetics (i.e. systems with negative Poisson's ratios) exhibit the unexpected feature of becoming fatter when stretched and narrower when compressed. This property is highly desirable as it imparts many beneficial effects on the material's macroscopic properties. Recent research suggests that in an idealised scenario, systems composed of connected 'rigid squares' can exhibit auxetic behaviour (Poisson's ratio = –1) due to a mechanism involving relative rotation of the squares. This paper shows through force-field based molecular modelling simulations that although 'rotating squares' are responsible for negative Poisson's ratios in various zeolite frameworks, in these real materials, the squares are not rigid and the auxeticity is not as pronounced as in the 'idealised' model. In view of this, a new model system made from connected 'semi-rigid' squares is proposed and analytical equations for the mechanical properties of this new model system are derived and discussed. It will be shown that the Poisson's ratios in this new model are highly dependent on the extent of rigidity of the squares and the direction of loading. It will also be shown that this new model provides a better description for the behaviour of auxetic zeolite frameworks than the original 'rotating rigid squares' model.

1 Introduction

Auxetics are systems which exhibit the property of expanding when pulled in a direction which is orthogonal to the direction of pulling. In the case of materials, the term 'auxetic' is equivalent to saying that the material exhibits a negative Poisson's ratio [1], but in recent years, this definition was extended to describe systems constructed at any scale which expand when pulled.

Although auxetics are not commonly encountered in everyday applications, it is well known that they can exist: the classical theory of elasticity states that isotropic three-dimensional materials may exhibit Poisson's ratios within the range $-1 \le \nu \le +1/2$; two-dimensional isotropic systems can exhibit Poisson's ratios within the range $-1 \le \nu \le +1$ [2]; whilst there are no bounds for the Poisson's ratios in anisotropic materials, and hence they can assume any positive or negative values in certain directions.

One of the earliest systems specifically designed to exhibit negative Poisson's ratios were Gibson and Ashby's two-dimensional re-entrant honeycombs deforming through flexure of the ribs [3] and Almgren's three-dimensional isotropic structure constructed from rods, hinges, and springs which maintains its aspect ratio in three dimensions, i.e. exhibits Poisson ratio's of –1 [4]. Since then, there was considerable development in the field of auxetics, and the property of lateral expansion when pulling has been predicted, discovered or deliberately introduced in various 'model structures' (e.g. the chiral macrostructure of Prall and Lakes [5, 6] or Wojciechowski's hard spheres model [7–9]) and in several classes of

* Corresponding author: e-mail: joseph.grima@um.edu.mt

naturally occurring or man-made materials ranging from microstructured materials such as foams [10–15], microporous polymers [16–18] to molecular-level auxetics such as polymers [1, 19–23], metals [24], silicates [25–33] and zeolites [34, 35].

All of these systems are characterised by having macro-, micro- or nanostructures with very particular geometric features which deform through very particular deformation mechanisms. Various geometric models, especially two-dimensional models which describe the behaviour of a particular cross-section of the material, have been developed in an attempt to explain the occurrence of negative Poisson's ratios. For example, 2D re-entrant hexagonal honeycomb models deforming through hinging or flexing have been developed and used to explain the auxeticity in foams [10–12] and hypothetical 'flexyne and reflexyne' nanostructured networked polymers [1], whilst 2D rotating polygon (e.g. rotating triangles [36], squares [37] and rectangles [15, 38, 39]) models have been developed and used to explain the auxeticity in foams [15], hypothetical nanostructured networked polymers [21], zeolites [34, 35] and silicates [32]. In this respect it is important to note, that:

(i) the same mechanism may operate at different scales of structure: for example, the same 'rotating triangles' model [36] has been applied to foams (the 'rotation of joints mechanism') [15] and molecular level systems such as the zeolite JBW [34];

(ii) more than one mechanism may be playing some role in generating auxetic behaviour in real systems: For example, it is being proposed that the auxetic behaviour in foams could be explained through 're-entrant' models [10–13], a 'missing ribs model' [14] or a 'rotation of joints' model [15] and that these models are not mutually exclusive.

Models meant to explain the occurrence of negative Poisson's ratios are extremely useful as they aid researchers understand more clearly the mechanisms by which negative Poisson's ratios can be achieved. However, most models have the drawback that they often represent idealised scenarios, whilst the behaviour of the real materials is much more complex. For example, whilst the 'rotating polygons' model can explain the presence of the auxetic effect in various classes of materials, they overestimate the auxeticity and fail to predict the dependence of the Poisson's ratios on the direction of loading [32, 34]. This problem can be rectified (at least in part) through further development of the models to include concurrent deformation mechanisms which could be taking place when the real material is subjected to mechanical loads.

This paper proposes and develops a new 'rotating semi-rigid squares' model to describe the predicted auxetic behaviour in zeolites with a 'rotating squares' nanostructure [34]. The new model is an extension of our earlier mathematical model describing the behaviour of 'rotating rigid squares' [37], with the difference that in the new model the squares will be allowed to deform apart from rotating relative to each other.

2 Existing 'rotating rigid squares' model and its suitability for modelling real materials

In 1999, it was reported that various zeolite frameworks including the SiO_2 equivalents of the zeolites THO, EDI and NAT in the Natrolite group are predicted to exhibit auxetic behaviour in the (001) plane), a behaviour which was reported to be due to a 'rotating squares' mechanism [40]. This 'rotating squares' mechanism (or, more generally, 'rotating rigid units' mechanism) is now recognised as one of the more important mechanisms for generating negative Poisson's ratios and in recent years, this mechanism has attracted considerable attention [15, 34, 37, 39–42].

The idealised version of the 'rotating squares' model may be constructed from squares of side length l connected together through hinges as illustrated in Fig. 1. The model requires the squares to remain perfectly rigid and deformations are restricted to rotation of the squares relative to each other (i.e. the structure deforms solely through changes in the parameter θ). This idealised system will not shear (i.e. the equivalent of having an infinite shear modulus) and will assume Poisson's ratios of -1 for loading in any direction in the Ox_1-Ox_2 plane, for any size of square and for any angle θ between the squares. In

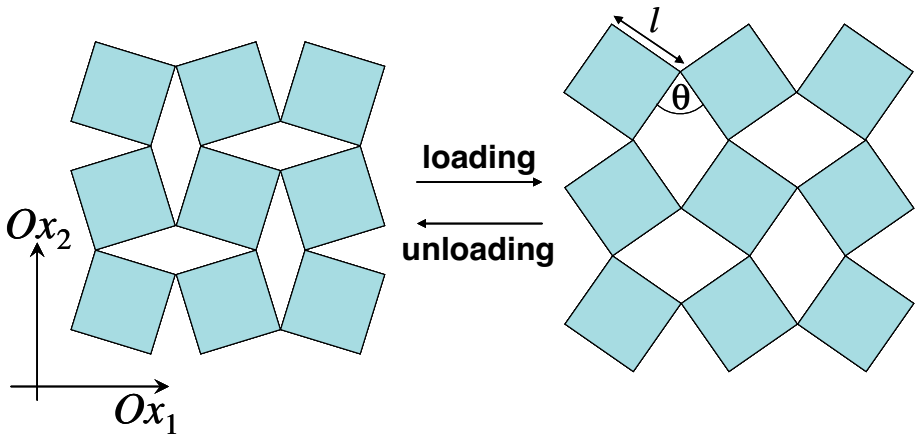

Fig. 1 (online colour at: www.pss-b.com) Idealised 'rotating rigid squares' model exhibiting Poisson's ratios of –1.

fact, assuming that the stiffness of the structure results solely from resistance to relative rotation of the squares (i.e. the squares are connected together through hinges which have a hinge constant K_h), the 'mechanical properties' of this idealised two dimensional system are completely described in terms of a (3 × 3) compliance matrix $\boldsymbol{S}$ which relates the applied stress σ to the resulting strain ε through $\varepsilon = \boldsymbol{S}\sigma$, i.e.:

$$\begin{pmatrix} \varepsilon_1 \\ \varepsilon_2 \\ \varepsilon_{12} \end{pmatrix} = \begin{pmatrix} s_{11} & s_{12} & s_{13} \\ s_{21} & s_{22} & s_{22} \\ s_{31} & s_{32} & s_{33} \end{pmatrix} \begin{pmatrix} \sigma_1 \\ \sigma_2 \\ \sigma_{12} \end{pmatrix}, \tag{1}$$

where in this particular case [37]:

$$\boldsymbol{S} = \frac{1}{E} \begin{pmatrix} 1 & 1 & 0 \\ 1 & 1 & 0 \\ 0 & 0 & 0 \end{pmatrix}, \tag{2}$$

where E is the equivalent of the Young's modulus of the structure (assuming thickness z in the third direction) which is given by:

$$E = K_h \frac{8}{zl^2} \frac{1}{[1 - \sin(\theta)]}. \tag{3}$$

However, in the real materials, this idealised behaviour is difficult to achieve, as illustrated by force-field based molecular modelling studies using the Burchart force-field (a specialised force-field containing bond and non-bond terms parameterised for use with silicates and zeolite frameworks [43]) on the SiO_2 equivalent of the zeolites THO, NAT and EDI.

The simulations of these systems were carried out using the software package Cerius^2 V3.0 (Accelrys Inc.) with the crystals aligned in global *XYZ* space such that the [001] crystal direction is always parallel to the global *Z*-axes and the [010] crystal direction aligned the global *YZ*-plane. An energy expression for each crystal was set up using the Burchart force-field [43] with non-bond terms added using the Ewald summation technique [44]. A geometry optimisation was performed to the default Cerius^2 high convergence criteria which include the requirement that the RMS force on each atom must be less than 0.001 kcal mol^{-1} Å^{-1}. The elastic constants were then simulated from the second derivative of the energy expression. Similar simulations were performed using the GULP code [45–47] developed by Prof. Julian Gale with parameters taken from the Catlow library [48–54].

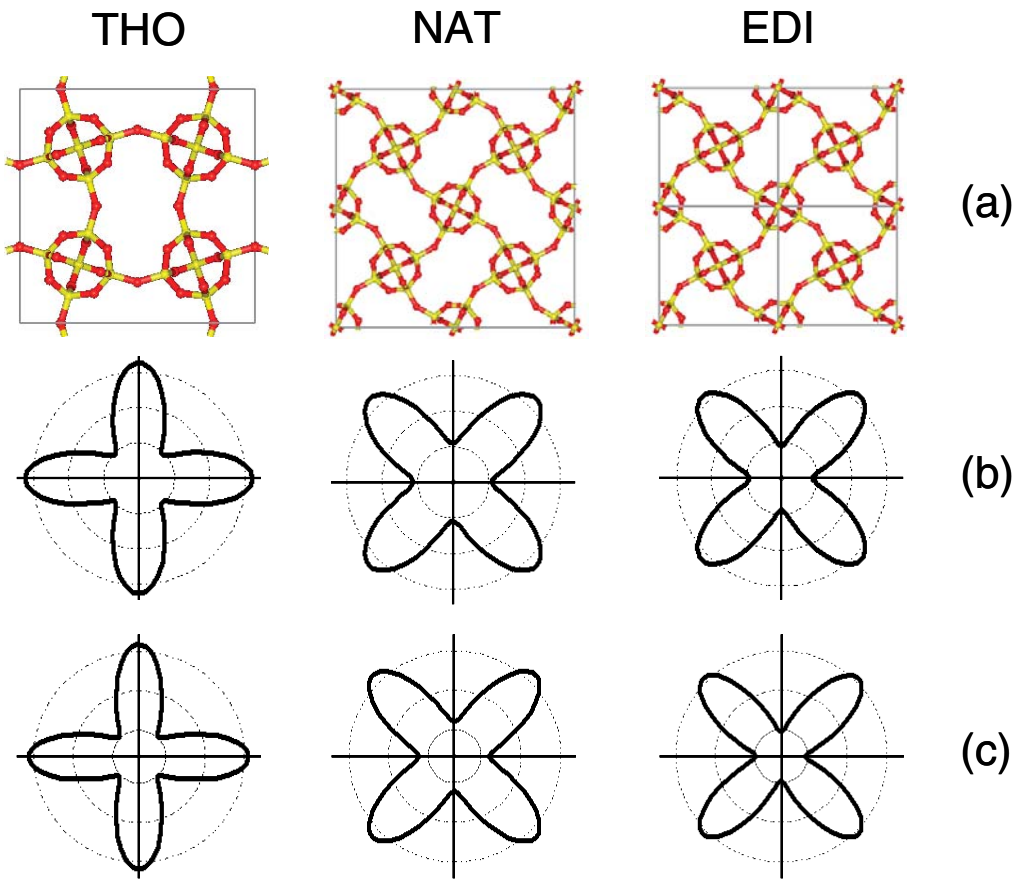

Fig. 2 (online colour at: www.pss-b.com) (a) (001) planes of minimum energy structures of the SiO_2 equivalents of THO, NAT and EDI as predicted by the Burchart force-field; (b) the Poisson's ratios for these systems in the (001) plane as predicted by the Burchart force-field; (c) the Poisson's ratios for these systems in the in the (001) plane as predicted by the Catlow library using the GULP.

These simulations suggest that although the crystal structure of the SiO_2 equivalents of THO, NAT and EDI in the (001) plane (the *XY*-plane) is very similar to the 'rotating squares' model (compare Figs. 1 and 2), the crystals are not as auxetic in the (001) plane as predicted by the 'idealised rotating squares' model, i.e. the Poisson's ratios in the (001) plane are not as negative as –1 (see Table 1 and Fig. 2). The simulations also suggest that in contrast to the idealised model, the auxeticity in the (001) plane of these SiO_2 zeolite equivalents depends on the direction of loading with maximum auxeticity occurring for loading in the [100] and [010] direction in the case of THO, and at 45° to these directions for NAT and EDI (see Fig. 2 and Table 1). This is very significant as these directions correspond to the major axis of the 'rotating squares' model (i.e. comparing Figs. 1 and 2, in the case of THO, the Ox_1 and Ox_2 directions of the analytical model in Fig. 1 correspond to the [100] and [010] crystal axis respectively, whilst in the case of NAT and EDI, the Ox_1 and Ox_2 directions of the analytical model correspond to the $[1\,\bar{1}0]$ and [110] directions respectively). Furthermore, these simulations suggest that the shear moduli in the (001) plane are not infinite as predicted by the analytical model for the idealised 'rotating rigid squares' model. (For example, in the case of THO, the Burchart force-field predicts that $G_{xy} \approx 50\%$ of E_x and E_y, see Table 1.)

Table 1 On- and off-axis mechanical properties of the SiO_2 equivalents of THO, NAT and EDI in the *xy*-plane (the (001) plane) as simulated using (a) Cerius[2] with the Burchart force-field and (b) GULP with the Catlow library. Note that the off-axis mechanical properties relate to the loading in the *xy*-plane at 45° to the *x*- and *y*-axis.

	on-axis mechanical properties					off-axis mechanical properties				
	ν_{xy}	ν_{yx}	E_x (GPa)	E_y (GPa)	G_{xy} (GPa)	$\nu_{xy}^{\zeta=45°}$	$\nu_{yx}^{\zeta=45°}$	$E_x^{\zeta=45°}$ (GPa)	$E_y^{\zeta=45°}$ (GPa)	$G_{xy}^{\zeta=45°}$ (GPa)
(a) results obtained using Cerius[2] with the Burchart force-field										
THO	−0.64	−0.65	32.6	33.0	14.6	−0.19	−0.19	23.7	23.7	46.3
NAT	−0.22	−0.22	23.1	23.1	46.3	−0.66	−0.66	31.4	31.4	14.8
EDI	−0.18	−0.18	24.0	24.0	46.4	−0.64	−0.64	33.3	33.3	14.6
(b) results obtained using GULP with the Catlow library										
THO	−0.63	−0.65	41.8	43.3	13.2	−0.01	−0.01	26.2	26.2	59.4
NAT	−0.07	−0.07	25.1	25.1	59.1	−0.67	−0.67	39.3	39.3	13.4
EDI	0.01	0.01	26.9	26.8	60.3	−0.63	−0.63	44.4	44.4	13.2

In an attempt to understand more clearly the atomic-level deformations that take place when these zeolites are mechanically loaded, we have performed force-field based simulations using the Burchart force-field where loads (in tension/compression and shear) were applied in directions which correspond to the major axis of the 'rotating squares model' i.e.:

(a) For loading in tension/compression in the direction equivalent to the Ox_1 direction (a direction of maximum auxeticity), the loads applied were:

$$\sigma = \begin{pmatrix} \cos(\zeta) & \sin(\zeta) & 0 \\ -\sin(\zeta) & \cos(\zeta) & 0 \\ 0 & 0 & 1 \end{pmatrix} \begin{pmatrix} \sigma & 0 & 0 \\ 0 & 0 & 0 \\ 0 & 0 & 0 \end{pmatrix} \begin{pmatrix} \cos(\zeta) & \sin(\zeta) & 0 \\ -\sin(\zeta) & \cos(\zeta) & 0 \\ 0 & 0 & 1 \end{pmatrix}^{\mathrm{T}} . \quad (4)$$

(b) For loading in shear the $Ox_1 - Ox_2$ plane, the loads applied were:

$$\sigma = \begin{pmatrix} \cos(\zeta) & \sin(\zeta) & 0 \\ -\sin(\zeta) & \cos(\zeta) & 0 \\ 0 & 0 & 1 \end{pmatrix} \begin{pmatrix} 0 & \sigma & 0 \\ \sigma & 0 & 0 \\ 0 & 0 & 0 \end{pmatrix} \begin{pmatrix} \cos(\zeta) & \sin(\zeta) & 0 \\ -\sin(\zeta) & \cos(\zeta) & 0 \\ 0 & 0 & 1 \end{pmatrix}^{\mathrm{T}} , \quad (5)$$

with $\sigma = -0.50, -0.25, ..., +0.50$ GPa, $\zeta = 0°$ in the case of THO and $\zeta = 45°$ in the case of NAT and EDI.

The simulations suggest very clearly that (see animations provided online at www.pss-b.com):

– The main deformation as a result of uniaxial loading in the Ox_1 direction is one where the molecular units which are being described as 'squares' rotate with respect to each other when subjected to these loads with the result that the structure 'opens up' when the load is increased (see Fig. 3); whilst

– Loading in shear (i.e. loads σ_{12}) primarily results in a deformation where the 'squares' change shape and assume the shape of a 'rectangle' with the result that the system now looks like that of the 'Type II rectangles structure' (using the nomenclature described in [55]).

In fact the simulations suggest that in the case of the SiO_2 equivalent of THO:

(a) Referring to Figs. 3a, 4 and Table 2a, a 1.0 GPa change in the load in the Ox_1 direction ($\Delta\sigma_1 = \Delta\sigma_x = 1.0$ GPa) will result in a large change in the angle between the squares (the angles θ change by 9.442°) whilst the other parameters change by very small amounts (the internal angles of squares and the angles between diagonals change by less than 1° and the lengths of the sides of the squares of the lengths of diagonals of the squares change by less than 0.7%);

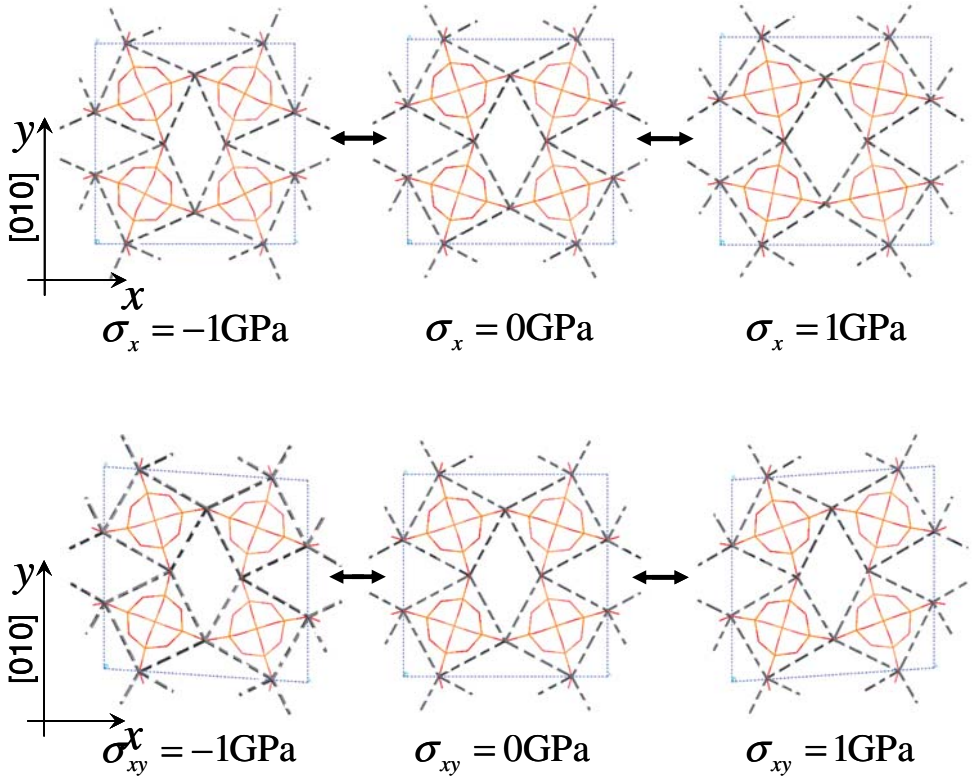

Fig. 3 (online colour at: www.pss-b.com) (001) planes of minimum energy structures of the SiO_2 equivalents of THO when subjected to (a) uniaxial loads in the *x*-direction, and (b) shear loads in the *xy*-plane as predicted by the Burchart force-field. (For an animated version of this figure see the supporting information provided for this article at www.pss-b.com.)

(b) Referring to Figs. 3b, 4 and Table 2b, a 1.0 GPa change in the shear load in the Ox_1-Ox_2 plane ($\Delta\sigma_{12} = \Delta\sigma_{xy} = 1.0$ GPa), will result in significant changes in the angles between the diagonals (the angles ϕ increase or decrease by 3.815°) but there are very little changes in the angles of the 'squares' (which now become rectangles) or in the length of the diagonals which only change by approx 0.3%. The change in the angles between the diagonals, ϕ, are accompanied by significant changes in the lengths of the sides of the 'squares' which increase/decrease by 3.3%, so as to become rectangles (an effect which can be explained in terms of the changes in angles ϕ between the diagonals).

Similar properties can be found in the SiO_2 equivalents of the zeolites NAT and EDI.

In view of all this we propose that a better model for the behaviour of these materials with a 'rotating squares' nanostructure is one where the squares are allowed to become rectangles [35]. This can be done by replacing the squares by their diagonals (see Fig. 4b and c), where the diagonals of the same square are connected through a hinge at their centres which has a hinge stiffness k_ϕ whilst diagonals of adjacent squares are connected through a hinge which has a hinge stiffness k_ψ. Referring to Fig. 4c, as a first approximation it will be assumed that the diagonals do not change their length (i.e. $l_d = |AC| = |BD|$ is constant) but the parameters ψ and ϕ can change concurrently.

Table 2(a) Gradients of plots of percentage changes (for lengths) and actual changes (for angles in degrees) vs. applied stress in the *x*-direction (in GPa). These values represent the change (percentage or actual) in the various lengths of sides/diagonals of squares etc. per GPa change in the applied stress in the *x*-direction. The parameters monitored are defined in Fig. 4.

N	% change in lengths of sides of squares*				% change in lengths of diagonals*	
	A_nB_n	B_nC_n	C_nD_n	D_nA_n	A_nC_n	B_nD_n
1	−0.150	0.464	−0.150	0.465	0.613	−0.299
2	−0.150	0.464	−0.150	0.464	0.613	−0.299
3	−0.150	0.464	−0.150	0.464	0.613	−0.299
4	−0.150	0.464	−0.150	0.464	0.613	−0.299

(*) Note: It may be useful to compare these % changes to the % changes in the cell parameters, where referring to Fig. 4, X_1 changes by 3.04% whilst X_2 changes by 1.95%.

n	changes in internal angles of the squares				changes in angles between diagonals of same square	changes in angles between squares/ diagonals of different squares	
	$A_nB_nC_n$	$B_nC_nD_n$	$C_nD_nA_n$	$D_nA_nB_n$	ϕ_n	θ_n	ψ_n
1	0.523	−0.523	0.522	−0.523	−0.352	9.442	9.272
2	0.523	−0.523	0.523	−0.523	−0.352	−9.442	8.568
3	0.523	−0.523	0.523	−0.523	−0.352	9.442	9.272
4	0.523	−0.523	0.523	−0.523	−0.352	−9.442	8.568

Table 2(b) Gradients of plots of percentage changes (for lengths) and actual changes (for angles in degrees) vs. applied shear stress in the *xy*-plane (in GPa). These values represent the change (percentage or actual) in the various lengths of sides/diagonals of squares etc. per GPa change in the applied shear stress in the *xy*-plane. The parameters monitored are defined in Fig. 4.

N	% change in lengths of sides of squares				% change in lengths of diagonals	
	A_nB_n	B_nC_n	C_nD_n	D_nA_n	A_nC_n	B_nD_n
1	−3.327	3.329	−3.327	3.329	−0.300	0.302
2	3.327	−3.330	3.328	−3.330	0.300	−0.301
3	−3.327	3.329	−3.327	3.329	−0.300	0.302
4	3.327	−3.330	3.327	−3.330	0.300	−0.301

n	changes in internal angles of the squares				changes in angles between diagonals of same square	changes in angles between squares/ diagonals of different squares	
	$A_nB_nC_n$	$B_nC_nD_n$	$C_nD_nA_n$	$D_nA_nB_n$	ϕ_n	θ_n	ψ_n
1	−0.345	0.345	−0.345	0.345	−3.815	0.009	0.009
2	0.344	−0.344	0.344	−0.344	3.815	−0.009	0.010
3	−0.345	0.345	−0.345	0.345	−3.815	0.009	0.009
4	0.344	−0.344	0.344	−0.344	3.815	−0.009	0.010

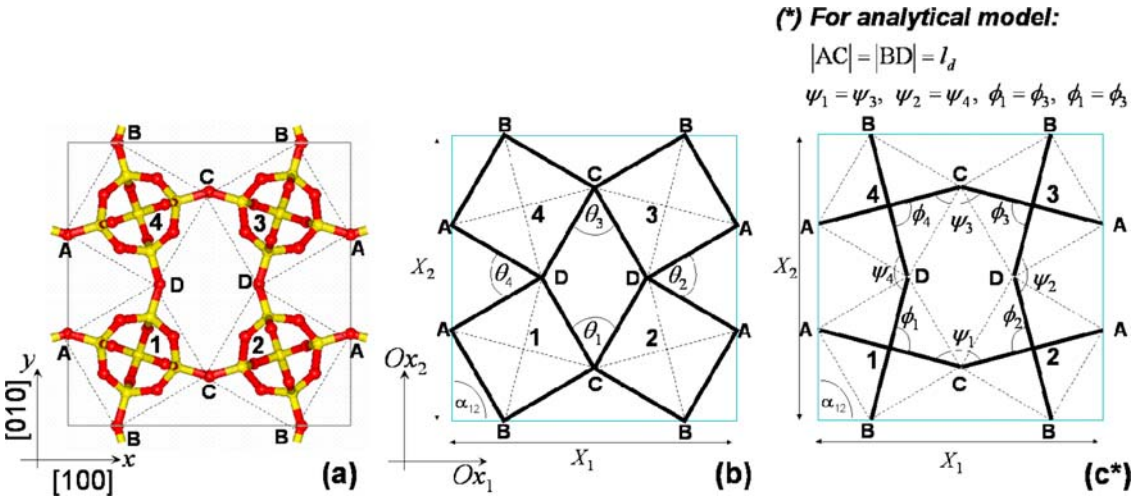

Fig. 4 (online colour at: www.pss-b.com) Definition of the variables monitored defined relative to THO (shown in (a)), with (b) the squares shown in bold, representing the original 'rotating squares' structure', and (c) the diagonals shown in bold, representing the new structure where the squares are replaced by their diagonals. Note that in the analytical model derived here, $\psi_1 = \psi_3$, $\psi_2 = \psi_4$, $\phi_1 = \phi_3$ and $\phi_2 = \phi_4$.

It should be noted that a similar model where deformability of squares was taken into account has also been proposed by Vasiliev et al. [42] where in this case, the deformability of square's diagonals was also taken into account. Thus, our model may be treated as a simplified version of this model [42], were the simplification introduced, i.e. that the diagonals do not change their length, is justified by the results of the molecular modelling simulations of the zeolite frameworks studied here.

3 New model: 'rotating semi-rigid squares'

3.1 Introduction

In this model we shall assume that the system is constructed from rod-like elements of length l_d (which represent the diagonals of squares of side length l) with a geometry as illustrated by the bold lines in Fig. 4c. It shall be assumed that the two diagonals within the same square are connected together by a hinge (i.e. similar to a pair of scissors) and are at an angle ϕ (= 90° initially) to each other. The diagonals from adjacent squares are also connected together by hinges and are at an angle ψ (= 90° + θ initially, θ being the angle between the squares).

In this derivation we shall assume that the structure may deform solely through changes in the angles ϕ and ψ. Referring to Fig. 4c, although there are four ϕ and four ψ angles per unit cell which are referred to as ϕ_1, ϕ_2, …, ϕ_4 and ψ_1, ψ_2, …, ψ_4, it can be shown that from geometry and symmetry considerations that the angles $\phi_1 = \phi_3$, $\phi_2 = \phi_4$, $\psi_1 = \psi_3$ and $\psi_2 = \psi_4$. Thus, in general the shape of this structure at various loads (in tension/compression or in shear) will depend on the four angle variables ϕ_1, ϕ_2, ψ_1 and ψ_2 defined as illustrated in Fig. 4, and the magnitudes of these angles at the various loads will depend on the relative stiffness of the hinges (i.e. on k_ϕ and k_ψ).

3.2 On-axis mechanical properties

In this section we derive the 3 × 3 compliance matrix $\boldsymbol{S}$ for the system illustrated in Fig. 4c, where $\boldsymbol{S}$ is defined as in Eq. (1). It may be deduced from the symmetry of the structure that loading in the Ox_i direction (i = 1, 2) will not change the unit cell angle α_{12} from π/2, i.e. $s_{31} = s_{32} = 0$. Thus, the compliance

matrix $\boldsymbol{S}$ will have four zero elements and the remaining five non-zero elements may be written in terms of the Poisson's ratios, Young's moduli and shear modulus as follows:

$$\boldsymbol{S} = \begin{pmatrix} s_{11} & s_{12} & 0 \\ s_{21} & s_{22} & 0 \\ 0 & 0 & s_{33} \end{pmatrix} = \begin{pmatrix} \dfrac{1}{E_1} & \dfrac{-\nu_{21}}{E_2} & 0 \\ \dfrac{-\nu_{12}}{E_1} & \dfrac{1}{E_2} & 0 \\ 0 & 0 & \dfrac{1}{G_{12}} \end{pmatrix}. \tag{6}$$

3.2.1 Uniaxial loading in the Ox_1 or Ox_2 directions

Because of symmetry, the mechanical properties for loading in the Ox_1 direction are identical to those for loading in the Ox_2 direction, i.e. $E_1 = E_2$ and $\nu_{12} = \nu_{21}$. In view of this, only the Young's moduli and Poisson's ratios for loading in Ox_2 will be derived. Furthermore, because of symmetry, loading in the Ox_1 or Ox_2 directions will result in deformations where the angles ϕ_1 and ϕ_2 remain equal to each other, i.e. $\mathrm{d}\phi_1 = \mathrm{d}\phi_2 = \mathrm{d}\phi$.

Referring to Fig. 4c, the projections of the unit cell in the Ox_1 and Ox_2 directions are given by:

$$X_1 = 2l_\mathrm{d} \sin\left(\frac{\psi_1}{2}\right) \qquad X_2 = 2l_\mathrm{d} \sin\left(\frac{\psi_2}{2}\right), \tag{7}$$

where from the geometric constraint that the sum of the interior angles of an n sided figure is equal to $(n-2)\,\pi$, the changes $\mathrm{d}\psi_i$ and $\mathrm{d}\phi_i$ in the angles ψ_i and ϕ_i are interrelated through:

$$2\,\mathrm{d}\psi_2 = 2\,\mathrm{d}\psi_1 + 2\,\mathrm{d}\phi_1 + 2\,\mathrm{d}\phi_2, \tag{8}$$

i.e.:

$$\mathrm{d}\psi_2 = \mathrm{d}\psi_1 + 2\,\mathrm{d}\phi. \tag{9}$$

A relationship between $\mathrm{d}\psi_1$ and $\mathrm{d}\phi$ for loading in the Ox_2 direction may be derived through considering the moments acting on the diagonals elements AC. As illustrated in Fig. 5, at equilibrium, the sum of moments acting on each diagonal is equal to zero, i.e.:

$$\sum M = M_\mathrm{A} + M_\mathrm{C} - M_\mathrm{O} = 0, \tag{10}$$

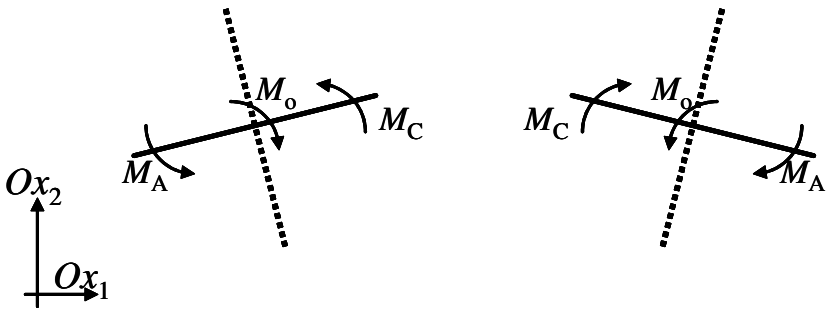

Fig. 5 Moments acting on diagonals AC.

where:

$$M_{\mathrm{A}} = M_{\mathrm{C}} = k_{\psi}\, \mathrm{d}\psi_1 , \qquad M_{\mathrm{O}} = k_{\phi}\, \mathrm{d}\phi . \tag{11}$$

Thus from Eqs. (10) and (11) we have:

$$k_{\phi}\, \mathrm{d}\phi = 2k_{\psi}\, \mathrm{d}\psi_1 \tag{12}$$

and hence:

$$\mathrm{d}\phi = 2\left(\frac{k_{\psi}}{k_{\phi}}\right)\mathrm{d}\psi_1 . \tag{13}$$

From Eqs. (9) and (13) the angle changes $\mathrm{d}\psi_1$ and $\mathrm{d}\phi$ may be expressed in terms of $\mathrm{d}\psi_2$ since:

$$\mathrm{d}\psi_2 = \mathrm{d}\psi_1 + 2\,\mathrm{d}\phi = \mathrm{d}\psi_1 + 4\left(\frac{k_{\theta}}{k_{\phi}}\right)\mathrm{d}\psi_1, \tag{14}$$

i.e.:

$$\mathrm{d}\psi_1 = \left[1 + 4\left(\frac{k_{\psi}}{k_{\phi}}\right)\right]^{-1} \mathrm{d}\psi_2 , \tag{15}$$

and

$$\mathrm{d}\phi = 2\left(\frac{k_{\psi}}{k_{\phi}}\right)\left[1 + 4\left(\frac{k_{\psi}}{k_{\phi}}\right)\right]^{-1} \mathrm{d}\psi_2 . \tag{16}$$

3.2.1 On-axis Poisson's ratios

The Poisson's ratio, ν_{21}, may be derived using:

$$\nu_{21} = -\frac{\mathrm{d}\varepsilon_1}{\mathrm{d}\varepsilon_2} = -\frac{\mathrm{d}X_1}{\mathrm{d}X_2}\cdot\frac{X_2}{X_1} , \tag{17}$$

where X_1 and X_2 are defined by Eq. (7) and $\mathrm{d}X_1$ and $\mathrm{d}X_2$ may be expressed in terms of $\mathrm{d}\psi_1$ and $\mathrm{d}\psi_2$ through:

$$\mathrm{d}X_1 = \left(\frac{\mathrm{d}X_1}{\mathrm{d}\psi_1}\right)\mathrm{d}\psi_1 = l_{\mathrm{d}}\cos\left(\frac{\psi_1}{2}\right)\mathrm{d}\psi_1 \tag{18}$$

and

$$\mathrm{d}X_2 = \left(\frac{\mathrm{d}X_2}{\mathrm{d}\psi_2}\right)\mathrm{d}\psi_2 = l_{\mathrm{d}}\cos\left(\frac{\psi_2}{2}\right)\mathrm{d}\psi_2 . \tag{19}$$

The term $\mathrm{d}X_1$ may be expressed in terms of $\mathrm{d}\psi_2$ through Eq. (15) to obtain:

$$\mathrm{d}X_1 = l_{\mathrm{d}}\left[1 + 4\left(\frac{k_{\psi}}{k_{\phi}}\right)\right]^{-1}\cos\left(\frac{\psi_1}{2}\right)\mathrm{d}\psi_2 . \tag{20}$$

Hence the Poisson's ratio ν_{21} may be obtained by substituting Eqs. (7), (18) and (19) into Eq. (17) to give:

$$\nu_{21}(=\nu_{12}) = -\left[1+4\left(\frac{k_\psi}{k_\phi}\right)\right]^{-1}\left\{\frac{\cos\left(\frac{\psi_1}{2}\right)\sin\left(\frac{\psi_2}{2}\right)}{\sin\left(\frac{\psi_1}{2}\right)\cos\left(\frac{\psi_2}{2}\right)}\right\} = -\cot\left(\frac{\psi_1}{2}\right)\tan\left(\frac{\psi_2}{2}\right)\left[1+4\left(\frac{k_\psi}{k_\phi}\right)\right]^{-1}. \quad (21)$$

At zero strain, (i.e. when $\psi_1 = \psi_2 = \psi$) this expression reduces to:

$$\nu_{21}(=\nu_{12}) = -\left[1+4\left(\frac{k_\psi}{k_\phi}\right)\right]^{-1}. \quad (22)$$

From this derivation it may be deduced that:

(1) In the limit of zero strain, the on-axis Poisson's ratios are within the range $-1 \le \nu_{21}, \nu_{12} < 0$ (from Eq. (22)).

(2) When $k_\phi \gg k_\psi$, $(k_\psi/k_\phi) \to 0$ and hence $\nu_{ij} \to -1$. In other words, as $k_\phi \to \infty$ the structure reduces to the idealised 'rotating rigid squares' system.

(3) The Poisson's ratios are strain dependent (from Eq. (21), at non-zero load, $\psi_1 \neq \psi_2$);

(4) The zero-strain Poisson's ratios are independent of the initial geometry and are only dependent on the relative stiffness of the two types of hinges (from Eq. (22)).

3.2.2 On-axis Young's moduli

The Young's modulus E_2 may be derived through the principle of conservation of energy. The unit cell contains four ψ_1, four ψ_2 'spring hinges' and four ϕ hinges. Thus the total work done when ψ_2 becomes $\psi_2 + \mathrm{d}\psi_2$ (and ψ_1, ϕ become $\psi_1 + \mathrm{d}\psi_1$ and $\phi + \mathrm{d}\phi$ respectively) is given by:

$$W = 4[\tfrac{1}{2}k_\theta(\mathrm{d}\psi_1)^2] + 4[\tfrac{1}{2}k_\theta(\mathrm{d}\psi_2)^2] + 4[\tfrac{1}{2}k_\phi(\mathrm{d}\phi)^2]. \quad (23)$$

Eq. (23) may be expressed in terms of $\mathrm{d}\psi_2$ through Eqs. (15) and (16) to obtain:

$$W = 4\left[\frac{1}{2}k_\psi\left(\left[1+4\left(\frac{k_\psi}{k_\phi}\right)\right]^{-1}\mathrm{d}\psi_2\right)^2\right] + 4\left[\frac{1}{2}k_\psi(\mathrm{d}\psi_2)^2\right] + 4\left[\frac{1}{2}k_\phi\left(2\left(\frac{k_\psi}{k_\phi}\right)\left[1+4\left(\frac{k_\psi}{k_\phi}\right)\right]^{-1}\mathrm{d}\psi_2\right)^2\right] = 4\left[\frac{k_\psi(k_\phi+2k_\psi)}{(k_\phi+4k_\psi)}\right](\mathrm{d}\psi_2)^2, \quad (24)$$

whilst the strain energy per unit volume is given by:

$$U = \frac{1}{2}E_2(\mathrm{d}\varepsilon_2)^2 = \frac{1}{2}E_2\left[\frac{\mathrm{d}X_2}{X_2}\right]^2 = \frac{1}{2}E_2\left[\left(\frac{\mathrm{d}X_2}{\mathrm{d}\psi_2}\right)\mathrm{d}\psi_2\frac{1}{X_2}\right]^2. \quad (25)$$

But from the principle of conservation of energy:

$$U = \frac{1}{V}W, \quad (26)$$

where V is the volume of the unit cell given by:

$$V = X_1X_2z, \quad (27)$$

where z is the thickness in the third dimension.

Thus from Eqs. (23) to (27) we obtain:

$$\frac{1}{2}E_2\left[\left(\frac{\mathrm{d}X_2}{\mathrm{d}\psi_2}\right)\mathrm{d}\psi_2\frac{1}{X_2}\right]^2=\frac{1}{X_1X_2z}\left[\frac{4k_\psi\left(k_\phi+2k_\psi\right)}{\left(k_\phi+4k_\psi\right)}\right](\mathrm{d}\psi_2)^2\,, \tag{28}$$

which simplifies to:

$$E_2=\left[\frac{8k_\psi\left(k_\phi+2k_\psi\right)}{\left(k_\phi+4k_\psi\right)}\right]\frac{X_2}{X_1z}\left(\frac{\mathrm{d}X_2}{\mathrm{d}\psi_2}\right)^{-2}\,, \tag{29}$$

i.e. by combining Eqs. (7), (19) and (29) we obtain:

$$E_2\,(=E_1)=\left[\frac{8k_\psi\left(k_\phi+2k_\psi\right)}{\left(k_\phi+4k_\psi\right)}\right]\frac{\sin\left(\frac{\psi_2}{2}\right)}{\sin\left(\frac{\psi_1}{2}\right)\cos^2\left(\frac{\psi_2}{2}\right)}\frac{1}{l_\mathrm{d}^2z}\,. \tag{30}$$

At zero strain (i.e. when $\psi_1=\psi_2=\psi$), Eq. (30) reduces to:

$$E_2\,(=E_1)=\left[\frac{8k_\psi\left(k_\phi+2k_\psi\right)}{\left(k_\phi+4k_\psi\right)}\right]\sec^2\left(\frac{\psi}{2}\right)\frac{1}{l_\mathrm{d}^2z}\,. \tag{31}$$

Note that this expression for the Young's modulus shows that the Young's modulus approaches ∞ when $\psi\to\pi$ which corresponds to the fully open structure.

3.2.3 On-axis shear modulus

The in-plane shear of this structure may also be derived through a conservation of energy approach. When the structure in Fig. 4c is subjected to a shear stress σ_{12}, the system will only deform through changes in the ϕ angles and the ψ angles remain constant. Thus, the distances between the centres of the squares (i.e. the points where the two diagonals of a square meet) remain constant and form the four vertices of a rhombus with the result that the ϕ angles are constrained to change in such a way that:

$$\mathrm{d}\phi_1=-\mathrm{d}\phi_2=\mathrm{d}\phi_3=-\mathrm{d}\phi_4\,. \tag{32}$$

It can also be shown geometrically that the unit cell angle α_{12} is equal to the angle ϕ_1 between the diagonals of 'square/rectangle 1', i.e.

$$\alpha_{12}=\phi_1\,. \tag{33}$$

But the shear strain ε_{12} may be approximated by the change in the angle α_{12}, i.e.:

$$\varepsilon_{12}\approx-\mathrm{d}\alpha_{12}=-\mathrm{d}\phi_1\,. \tag{34}$$

Thus, from the principle of conservation of energy, the strain energy per unit volume is related to the work done by the four 'ϕ' hinges through:

$$\frac{1}{2}G_{12}\varepsilon_{12}^2=\frac{1}{V}4\left[\frac{1}{2}k_\phi|\mathrm{d}\phi|^2\right], \tag{35}$$

where

$$|\mathrm{d}\phi|=|\mathrm{d}\phi_1|=|\mathrm{d}\phi_2|=|\mathrm{d}\phi_3|=|\mathrm{d}\phi_4|\,, \tag{36}$$

and where V is the volume of the unit cell given by:

$$V = X_1 \sin(\alpha_{12})\, X_2 z = X_1 \sin(\phi_1)\, X_2 z \ , \tag{37}$$

i.e. by substituting Eqs. (34), (36) and (37) into Eq. (35):

$$G_{12} = \frac{4k_\phi}{V}\frac{|\mathrm{d}\phi|^2}{\varepsilon_{12}^2} = 4k_\phi \frac{1}{X_1 X_2 \sin(\phi_1)\, z}\frac{|\mathrm{d}\phi|^2}{|\mathrm{d}\phi|^2} = 4k_\phi \frac{4k_\phi}{X_1 X_2 \sin(\phi_1)\, z} \ . \tag{38}$$

Thus since $\psi_1 = \psi_2 = \psi$ and initially $\phi_1 = \pi/2$, by substituting Eq. (7) into Eq. (38):

$$G_{12} = k_\phi \frac{1}{z}\left[l_\mathrm{d} \sin\left(\frac{\psi}{2}\right)\right]^{-2} . \tag{39}$$

It is important to note that Eq. (39) suggests that G_{12} becomes infinite if either (1) k_ϕ is infinite (which relates to the rigid rotating hinged squares tessellation, or, (2) if ψ is $0 \pm 2n\pi$ which relates to the fully collapsed structure.

3.2.4 Summary

To summarise, the mechanical properties of this system are completely defined by the 3×3 compliance matrix $\boldsymbol{S}$ where:

$$\boldsymbol{S} = \begin{pmatrix} \dfrac{1}{E_1} & \dfrac{-\nu_{21}}{E_2} & 0 \\ \dfrac{-\nu_{12}}{E_1} & \dfrac{1}{E_2} & 0 \\ 0 & 0 & \dfrac{1}{G_{12}} \end{pmatrix}, \tag{40}$$

where

$$\nu_{12} = \nu_{21} = -\left[1 + 4\left(\frac{k_\psi}{k_\phi}\right)\right]^{-1} , \tag{41}$$

$$E_1 = E_2 = \left[\frac{8k_\psi\left(k_\phi + 2k_\psi\right)}{\left(k_\phi + 4k_\psi\right)}\right]\sec^2\left(\frac{\psi}{2}\right)\frac{1}{l_\mathrm{d}^{\,2} z} , \tag{42}$$

$$G_{12} = k_\phi \frac{1}{z}\left[l_\mathrm{d} \sin\left(\frac{\psi}{2}\right)\right]^{-2} . \tag{43}$$

3.3 Off-axis mechanical properties

The in-plane off-axis mechanical properties may be calculated using standard axis transformation technique on the parent 4th rank tensor of the compliance matrix. In particular, for systems such as the one discussed here where the compliance matrix has four zero elements $s_{13} = s_{23} = s_{31} = s_{32} = 0$, the off-axis

mechanical properties for a transformation involving an axis rotation by an angle ζ around the third direction are given by:

$$E_1^{\zeta} = \left[\frac{m^4}{E_1} + \frac{n^4}{E_2} - m^2 n^2 \left(2\frac{\nu_{12}}{E_1} - \frac{1}{G_{12}} \right) \right]^{-1},$$

$$\nu_{12}^{\zeta} = E_1^{\zeta} \left[(m^4 + n^4) \frac{\nu_{12}}{E_1} - m^2 n^2 \left(\frac{1}{E_1} + \frac{1}{E_2} - \frac{1}{G_{12}} \right) \right], \tag{44}$$

$$G_{12}^{\zeta} = \left[(m^4 + n^4) \frac{1}{G_{12}} + 2m^2 n^2 \left(2\frac{1}{E_1} + 4\frac{\nu_{12}}{E_1} + 2\frac{1}{E_2} + \frac{1}{G_{12}} \right) \right]^{-1},$$

where $m = \cos(\zeta)$ and $n = \sin(\zeta)$.

These equations show very clearly that in this case, unlike in the idealised 'rotating rigid squares' model, the mechanical properties and in particular ν_{12}^{ζ} are functions of ζ, i.e. they depend on the direction of loading. Plots of ν_{12}^{ζ} vs. ζ for $l_d = 2$, $\psi = 145°$ are given in Fig. 6. These plots suggest that:

1. Maximum auxeticity is achieved for loading the structure on-axis, i.e. in the Ox_1 or Ox_2 directions;

2. In the case when $k_\phi \gg k_\psi$, the Poisson's ratio approaches -1, a value which is independent of the direction of loading. This is due to fact that in such scenarios the squares become 'rigid'.

3. Although according to this model, the on-axis Poisson's ratios are always negative (Eq. (22)) suggests that $-1 \le \nu_{21}, \nu_{12} < 0$), the off-axis Poisson's ratios may be positive, in which case, the maximum positive Poisson's ratios are achieved for loading at 45° to the Ox_i directions.

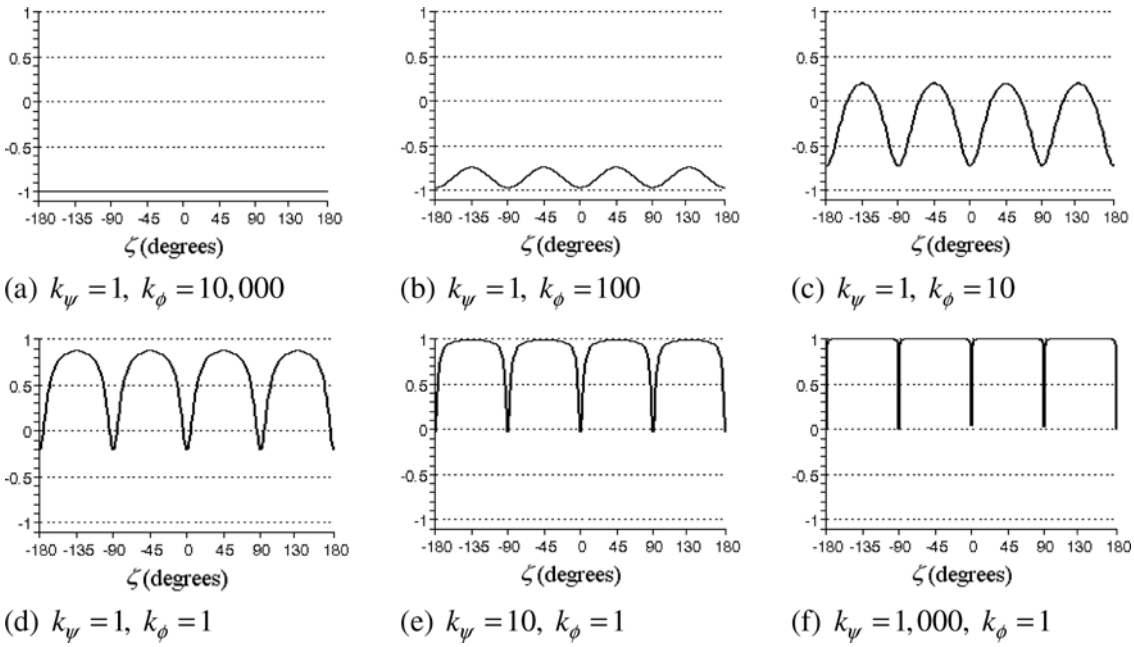

Fig. 6 Off-axis plots for various combinations of k_ϕ and k_ψ with $\psi = 145°$.

4 Discussion: The suitability of the new 'rotating semi-rigid squares' model for modelling real materials

The model presented above shows that a very simple modification of the idealised 'rotating rigid squares' model where the squares are allowed to deform by giving them an additional degree of freedom (the angle between their diagonals) results in very significant changes in the mechanical properties, and in particular the Poisson's ratios. In this new model, the Poisson's ratios ν_{12}^{ζ} in the plane of the structure are scale independent but depend on the ratio of the stiffness constants k_ϕ and k_ψ, on the geometric parameter ψ and on the direction of loading (see Eqs. (22) and (44)). Note that the dependence of ν_{12}^{ζ} on the geometric parameter ψ arises from the fact that $E_1 = E_2$ and G_{12} are functions of ψ (the angle between diagonals of adjacent squares), l_d (the length of the diagonals) and z (the thickness in the third dimension), and when these are substituted into the equation for ν_{12}^{ζ} Eq. (44), l_d and z cancel out (hence confirming that the Poisson's ratios are scale independent) but ψ remains a variable for the equation of ν_{12}^{ζ}. Note that similar conclusions may be drawn from Vasiliev et al.'s model [42] which also takes into account the deformability of the diagonals of the squares.

The model presented here (from Eqs. (31) and (39)) also suggests that the stiffness constants k_ϕ and k_ψ may be re-written in terms of the Young's moduli $E_1 = E_2 = E$ the shear modulus G_{12} and the geometric parameter ψ by solving Eqs. (31) and (39) simultaneously. This enables a direct comparison between the analytical model for the Poisson's ratios derived here and the Poisson's ratios of materials with a 'rotating squares geometry' obtained from experimental data or molecular modelling predictions. For example, in the case of the SiO_2 equivalent of THO, force-field based simulations using the Burchart force-field produce values of E (= average of E_x and E_y) = 32.8 GPa, $G_{12} = G_{xy}$ = 14.6 GPa and ψ = 146.48° (the average angle ψ) which when substituted into Eqs. (31) and (39) suggest that $k_\psi/k_\phi = 1/37.43$. Thus, assuming that $k_\psi = 1$ and $k_\phi = 37.43$, and substituting these values into Eqs. (22), (31), (39) and (44), one obtains an expression for $\nu_{12}^{\zeta}(\mathrm{AM})$, the off-axis Poisson's ratio ν_{12}^{ζ} as predicted by the analytical model, which can be compared to $\nu_{xy}^{\zeta}(\mathrm{MM})$, the off-axis Poisson's ratio ν_{xy}^{ζ} obtained by transforming the compliance matrix of the SiO_2 equivalent of THO as simulated by the Burchart force-field. A graphical comparison of $\nu_{12}^{\zeta}(\mathrm{AM})$ and $\nu_{xy}^{\zeta}(\mathrm{MM})$ is shown in Fig. 7, and this clearly shows that the new model can predict the off-axis Poisson's ratios extremely well although it overestimates the extent of auxeticity (see Fig. 7 and Table 3). In particular the analytical model correctly predicts the directions of maximum and minimum auxeticity (i.e. maximum auxeticity for loading on-axis, minimum for loading at 45° off-axis). Similar results were obtained for NAT and EDI, although in this case, the Ox_1 and Ox_2 axis of the analytical model were set parallel to the $[1\bar{1}0]$ and $[110]$ crystal directions respectively so as to align the 'analytical model' with the 'molecular model'.

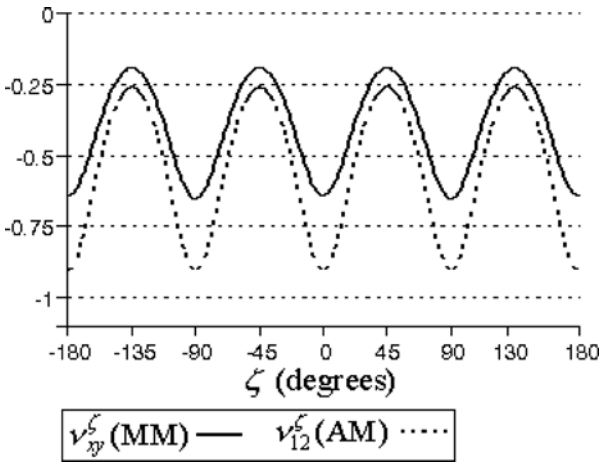

Fig. 7 A comparison of the off-axis Poisson's ratios ν_{12}^{ζ} for THO as predicted by the analytical model (AM) and molecular modelling (MM). Molecular modelling results were obtained using the Burchart force-field.

Table 3 Comparison of the on-axis ($\zeta = 0°$) and 45° off-axis ($\zeta = 45°$) Poisson's ratio for THO obtained from molecular modelling using the Burchart force-field (MM), as predicted from the analytical model (AM) and as predicted by the idealised 'rotating rigid squares' model. (Note: For AM, $k_\phi = 37.43$ and $k_\theta = 1$, and have arbitrary units.)

	ν_{xy}^{ζ}(MM)	ν_{12}^{ζ}(AM)	ν_{12}^{ζ} for the idealised 'rotating rigid squares'
$\zeta = 0°$	−0.65	−0.90	−1
$\zeta = 45°$	−0.19	−0.26	−1

All this is very significant as it suggests that a very simple 'geometric model' has been set up which can reproduce reasonably well the behaviour of 'real materials' and the manner how they can achieve the very useful property of having a negative Poisson's ratio. In fact, the new model can reproduce the properties of the 'real materials' to such detail that it can also account for the dependence of the Poisson's ratio on the direction of loading. However, there is still room for improvement in this analytical model since the auxeticity is still being overestimated (although there is a significant improvement over the original 'rotating rigid squares' model, see Table 3). Nevertheless, given the complexity of the zeolites' nanostructure and the simplicity of the analytical model, it can be concluded that the model gives a reasonable description of the mechanical properties of these three zeolites.

5 Conclusions

In this work, in an attempt to describe the predicted auxetic properties of various zeolite frameworks, we have presented a simple extension of the original 'rotation of rigid squares' model to include the possibility that the squares change shape concurrently to rotating with respect to each other, by simply introducing an additional degree of freedom (the angle between the diagonals of the squares).

We have shown that in such a model, in accordance with other work [42], the Poisson's ratios are no longer equal to −1, independently of the size of the squares, the initial angles between the squares and the direction of loading but become highly dependent on:

– The relative extent of 'deformation of the squares' vs. 'relative rotation of the squares' (in our case defined through the ratio of the stiffness constants k_ψ/k_ϕ);

– The direction of loading, with maximum auxeticity observed for loading 'on-axis';

– The initial angles between the squares (which in this model is represented by the angle ψ, the angle between the diagonals of adjacent squares).

Furthermore, we have shown that this new model can provide a much better representation of the Poisson's of the SiO_2 equivalents of zeolites with a 'rotating squares nanostructure', and in particular the model is able to reproduce the profile of the 'off-axis' Poisson's ratios plot of these 'real materials' extremely well. This is very significant as we are now able to understand much more clearly how negative Poisson's ratios can be exhibited in molecular frameworks of naturally occurring materials.

Acknowledgements The authors would like to take the opportunity to show their appreciation to Prof. Julian D. Gale of the Curtin University of Technology for supplying the GULP program. They also gratefully acknowledge the work of Trevor G. Chircop Bray and Lara Trapani of the University of Malta.

References

[1] K. E. Evans, M. A. Nkansah, I. J. Hutchinsonm, and S. C. Rogers, Nature **353**, 124 (1991).
[2] K. W. Wojciechowski, J. Phys. Soc. Jpn. **72**, 1819 (2003).
[3] L. J. Gibson, M. F. Ashby, G. S. Schajer, and C. I. Robertson, Proc. R. Soc. Lond. A **382**, 25 (1982).
[4] R. F. Almgren, J. Elast. **15**, 427 (1985).
[5] D. Prall and R. S. Lakes, Int. J. Mech. Sci. **39**, 305 (1997).
[6] A. Spadoni, M. Ruzzene and F. Scarpa, phys. stat. sol. (b) **242**, 695–709 (2005).

[7] K. W. Wojciechowski, Mol. Phys. **61**, 1247 (1987).
[8] K. W. Wojciechowski and A. C. Branka, Phys. Rev. A **40**, 7222 (1989).
[9] K. W. Wojciechowski, J. Phys. A, Math. Gen. **36**, 11765 (2003b).
[10] R. S. Lakes, Science **235**, 1038 (1987).
[11] K. E. Evans, M. A. Nkansah, and I. J. Hutchinson, Acta Metall. Mater. **2**, 1289 (1994)
[12] J. B. Choi and R. S. Lakes, J. Compos. Mater. **29**, 113 (1995)
[13] N. Chan and K. E. Evans, J. Cellular Plast. **34**, 231 (1998).
[14] C. W. Smith, J. N. Grima, and K. E. Evans, Acta Mater. **48**, 4349 (2000)
[15] J. N. Grima, A. Alderson, and K. E. Evans, J. Phys. Soc. Jpn. **74**, 1341–1342 (2005)
[16] K. E. Evans and B. D. Caddock, J. Phys. D, Appl. Phys. **22**, 1883 (1989).
[17] A. Alderson and K. E. Evans, J. Mater. Sci. **30**, 3319 (1995).
[18] A. Alderson and K. E. Evans, J. Mater. Sci. **32**, 2797 (1997).
[19] R. H. Baughman and D. S. Galvao, Nature **365**, 635 (1993).
[20] C. B. He, P. W. Liu, and A. C. Griffin, Macromolecules **31**, 3145 (1998).
[21] J. N. Grima and K. E. Evans, Chem. Commun. 1531 (2000).
[22] J. N. Grima, J. J. Williams, and K. E. Evans, Chem. Commun. **32**, 4065 (2005).
[23] G. Y. Wei, phys. stat. sol. (b) **242**, 742–748 (2005).
[24] R. H. Baughman, J. M. Shacklette, A. A. Zakhidov, and S. Stafstrom, Nature **392**, 362 (1998).
[25] A. Yeganeh-Haeri, D. J. Weidner, and D. J. Parise, Science **257**, 650 (1992).
[26] N. R. Keskar and J. R. Chelikowsky, Phys. Rev. B **46**, 1 (1992).
[27] H. Kimizuka, H. Kaburaki, and Y. Kogure, Phys. Rev. Lett. **84**, 5548 (2000).
[28] A. Alderson and K. E. Evans, Phys. Rev. Lett. **89**, 225503 (2002).
[29] H. Kimizuka, H. Kaburaki, and Y. Kogure, Phys. Rev. B **67**, 024105 (2003).
[30] A. Alderson, K. L. Alderson, K. E. Evans, J. N. Grima, and M. Williams, J. Met. Nano. Mater. **23**, 55 (2004).
[31] A. Alderson, K. L. Alderson, K. E. Evans, J. N. Grima, M. Williams, and P. J. Davies, phys. stat. sol. (b) **242**, 499–508 (2005).
[32] J. N. Grima, R. Gatt, A. Alderson, and K. E. Evans, J. Mater. Chem. **15**, 4003–4005 (2005).
[33] J. N. Grima, R. Gatt, A. Alderson, and K. E. Evans, Mater. Sci. Eng. A **423**, 219–224 (2006).
[34] J. N. Grima, R. Jackson, A. Alderson, and K. E. Evans, Adv. Mater. **12**, 1912 (2000).
[35] J. N. Grima, PhD Thesis, University of Exeter (Exeter, UK, 2000).
[36] J. N. Grima and K. E. Evans, J. Mater. Sci. **41**, 3193–3196 (2006).
[37] J. N. Grima and K. E. Evans, J. Mater. Sci. Lett. **19**, 1563 (2000).
[38] A. Alderson, K. L. Alderson, K. E. Evans, J. N. Grima, M. R. Williams, and P. J. Davies, Comp. Met. Sci. and Technol. **10**, 117–126 (2004).
[39] J. N. Grima, A. Alderson, and K. E. Evans, phys. stat. sol. (b) **242**, 561–575 (2005).
[40] J. N. Grima, A. Alderson, and K. E. Evans, Zeolites with negative Poisson's ratios, Paper presented at the RSC 4th International Materials Conference (MC4), Dublin, Ireland, P81, July 1999.
[41] Y. Ishibashi and M. J. Iwata, J. Phys. Soc. Jpn. **69**, 2702 (2000).
[42] A. A. Vasiliev, S. V. Dmitriev, Y. Ishibashi, and T. Shigenari, Phys. Rev. B **65**, 094101 (2002).
[43] E. de Vos Burchart, Studies on Zeolites, Molecular Mechanics, Framework Stability, and Crystal Growth, Ph.D. Thesis, Technische Universiteit Delft (1992).
[44] P. P. Ewald, Ann. Phys. **64**, 253 (1921).
[45] J. D. Gale, JCS Faraday Trans. **93**, 629 (1997).
[46] J. D. Gale, Phil. Mag. B **73**, 3 (1996).
[47] J. D. Gale and A. L. Rohl, Mol. Simul. **29**, 291 (2003).
[48] M. J. Sanders, M. J. Leslie, and C. R. A. Catlow, J. Chem. Soc., Chem. Commun. 1271 (1984).
[49] R. A. Jackson and C. R. A. Catlow, Mol. Simul. **1**, 207–224 (1988).
[50] K. P. Schroder, J. Sauer, M. Leslie, C. R. A. Catlow, and J. M. Thomas, Chem. Phys. Lett. **188**, 320 (1992).
[51] J. D. Gale and N. J. Henson, JCS Faraday Trans. **90**, 3175 (1994).
[52] A. Jentys and C. R. A. Catlow, Catal. Lett. **22**, 251–257 (1993).
[53] D. W. Lewis, C. R. A. Catlow, G. Sankar, and S. W. Carr, J. Phys. Chem. **99**, 2377–2383 (1995).
[54] C. J. J. den Ouden, R. A. Jackson, C. R. A. Catlow, and M. F. M. Post, J. Phys. Chem. **94**, 5286–5290 (1990).
[55] J. N. Grima, R. Gatt, A. Alderson, and K. E. Evans, J. Phys. Soc. Jpn. **74**, 2866–2867 (2005).

